

The impact of disk-locking on convective turnover times of low-mass pre-main sequence and main sequence stars

N. R. Landin^{1,2}, L. T. S. Mendes^{3,2}, L. P. R. Vaz², and S. H. P. Alencar²

¹ Universidade Federal de Viçosa, Campus UFV Florestal, CEP 35690-000 – Florestal, MG, Brazil
e-mail: nlandin@ufv.br

² Depto. de Física, Universidade Federal de Minas Gerais, C.P.702, 31270-901 – Belo Horizonte, MG, Brazil

³ Depto. de Engenharia Eletrônica, Universidade Federal de Minas Gerais, C.P.702, 31270-901 – Belo Horizonte, MG, Brazil

Received ; accepted

ABSTRACT

Aims. The impact of disk-locking on the stellar properties related to magnetic activity from the theoretical point of view is investigated. **Methods.** We use the ATON stellar evolution code to calculate theoretical values of convective turnover times (τ_c) and Rossby numbers (Ro , the ratio between rotation periods and τ_c) for pre-main sequence (pre-MS) and main sequence (MS) stars. We investigate how τ_c varies with the initial rotation period and with the disk lifetime, using angular momentum conserving models and models simulating the disk-locking mechanism. In the latter case, the angular velocity is kept constant, during a given locking time, to mimic the magnetic locking effects of a circumstellar disk.

Results. The local convective turnover times generated with disk-locking models are shorter than those obtained with angular momentum conserving models. The differences are smaller in the early pre-MS, increase with stellar age and become more accentuated for stars with $M \geq 1 M_\odot$ and ages greater than 100 Myr. Our new values of τ_c were used to estimate Ro for a sample of stars selected from the literature in order to investigate the rotation-activity relationship. We fit the data with a two-part power-law function and find the best fitting parameters of this relation.

Conclusions. The differences we found between both sets of models suggest that the star's disk-locking phase properties affect its Rossby number and its position in the rotation-activity diagram. Our results indicate that the dynamo efficiency is lower for stars that had undergone longer disk-locking phases.

Key words. stellar evolution – convection – rotation – pre-main sequence – magnetic activity – disk-locking

1. Introduction

The convective turnover time is a typical timescale for convective motions of the stars' conductive plasma, responsible for transportation of a fraction of the energy in some types of stars, like the low-mass ones. When different parts of a magnetic star rotate differentially, the interaction between convective motions and differential rotation produces the dynamo effect (as proposed by Parker 1955) that keeps and regenerates stellar magnetic fields. In solar type stars, such fields are thought to be created and amplified at the tachocline, a thin shear layer between the radiative core and the convective envelope, first defined by Spiegel & Zahn (1992). This mechanism is supposed to drive stellar magnetic activity, expressed as a variety of observable phenomena like coronal heating, star spots, activity cycles, flares and chromospheric and coronal emissions. For solar-like stars, it is believed that stellar magnetism and rotation are regulated by a dynamo process called the α - Ω dynamo (Mohanty & Basri 2003), in which the poloidal and toroidal field components sustain themselves through a cyclic feedback process (Nelson 2008). Nowadays, the connection between magnetic activity and rotation is well established, and Skumanich (1972) was the first to suggest that the rotation-activity relation is a consequence of the dynamo action and showed that the stellar angular velocity, Ω , decreases with age as $t^{-1/2}$. The rotation-magnetic activity relation has been widely used to investigate stellar magnetism. It

is expressed by the relation between the stellar rotation rate (the projected rotational velocity in the line of sight or the rotation period) and some indicator of magnetic activity, such as the unsigned average large-scale surface fields ($\langle |B_V| \rangle$) or the fractional X-ray and H α luminosities, also known as coronal (L_X/L_{bol}) and chromospheric ($L_{H\alpha}/L_{bol}$) activity indicators, respectively. As shown by Noyes et al. (1984), this relationship is better understood in terms of the Rossby number, Ro (the ratio between rotation period, P_{rot} , and the local convective turnover time, τ_c), than in terms of P_{rot} . Pizzolato et al. (2003) showed for the first time that the rotation-magnetic activity relation was characterised by the existence of two distinct regions: the saturated region (formed by fast rotators - $P_{rot} \leq 2$ days) and the unsaturated region (composed by slow rotators - $P_{rot} > 2$ days). L_X/L_{bol} (or another magnetic activity indicator) increases as Ro decreases down to a saturation threshold value, $Ro_{sat} \sim 0.1$, and remains constant at a saturation level, $(L_X/L_{bol})_{sat} \sim 10^{-3}$, for $Ro < Ro_{sat}$ (Wright et al. 2011, 2018). The causes of saturation are still unclear. This relation became a powerful tool to study stellar magnetism and is based on a general power-law function of the form $L_X/L_{bol} \propto Ro^\beta$, where β is a parameter to be adjusted with observations. Values of β usually found in the literature are $\beta = -2$ (Pizzolato et al. 2003), $\beta = -2.7 \pm 0.13$ (Wright et al. 2011), $\beta = -1.38 \pm 0.14$ (Vidotto et al. 2014), $\beta = -2.3^{+0.4}_{-0.6}$ (Wright et al. 2018), $\beta = -1.40 \pm 0.10$ (See et al. 2019) and $\beta = -2.4 \pm 0.1$ (Landin et al. 2023).

Describing the rotation-magnetic activity relation in terms of the Rossby number makes clear its connection with the stellar dynamo theory, as the dynamo number (N_D , the efficiency of the dynamo in the mean-field dynamo theory) is proportional to the inverse square of the Rossby number ($N_D \propto Ro^{-2}$). Consequently, the dynamo efficiency increases as Ro decreases. As Ro plays an important role in the stellar magnetic activity studies, determinations of τ_c are of fundamental interest, since they cannot be directly measured. They can be obtained either semi-empirically (Noyes et al. 1984, Pizzolato et al. 2003) or theoretically by stellar evolution models (Kim & Demarque 1996, Landin et al. 2010). For a given stellar mass and age, the convective turnover time varies significantly with the radial location. The location mostly used in the literature to determine local convective turnover times is one half a mixing length above the base of the convective zone (Noyes et al. 1984). This standard location coincides with the tachocline for partially convective stars, but it is not suitable for fully convective stars, in which there is no tachocline. In the Mixing Length Theory, the adjustable mixing length parameter, ℓ , is scaled with the pressure scale height H_p as $\ell = \alpha H_p$ (α is the convection efficiency) and, during the fully convective phase, the modelled value of H_p at the base of the convective zone is very high, and so is the mixing length. Consequently, the standard location where τ_c should be calculated becomes larger than the stellar radius for fully convective configurations ($M \leq 0.3 M_\odot$ at any evolutionary stage and $M > 0.3 M_\odot$ before developing the radiative core), making τ_c calculations unfeasible through this standard prescription. In order to overcome this problem, Landin et al. (2023) developed a method to obtain the location (r) where to calculate τ_c in terms of H_p , allowing the theoretical determination of τ_c of fully convective stars in a self consistent way with the traditional location prescribed by Noyes et al. (1984). For 10 selected ages in the range of $6.0 \leq \log(t/\text{yr}) \leq 10.14$, Landin et al. (2023) analysed how the standard location r/H_p varied with stellar mass for partially convective stars, linearly fitted r/H_p as a function of the stellar mass and extrapolated it for fully convective stars. These linear fits of r/H_p as a function of mass were introduced in the ATON stellar evolution code as alternative locations to the standard τ_c calculation whenever r is larger than the stellar radius. Otherwise, the standard location is adopted.

Most, if not all, low-mass pre-main sequence (pre-MS) stars exhibit some manifestation of magnetic fields (Donati & Landstreet 2009). As they miss a tachocline in the beginning of their pre-MS phase, the α - Ω dynamo, which is an interface dynamo, is not supposed to be operating in this very early evolutionary phase. So, the observed magnetic activity in these stars should be produced by another kind of dynamo process, like a distributed dynamo, as suggested by Durney et al. (1993). The characteristic shape of the rotation-activity relation exhibited by main sequence (MS) stars is not observed for pre-MS stars (Flaccomio et al. 2003). The latter are seen only in the saturated region and show a considerable dispersion in magnetic activity levels (Preibisch et al. 2005). The fact that fully convective (pre-MS and MS) stars are preferably found in the saturated region, while solar-like (partially convective) stars are found in both regions, reinforces the idea that the dynamo operating in partially and fully convective stars are different. However, observations by Wright & Drake (2016) and Wright et al. (2018) indicate that partially and fully convective stars follow the same rotation-activity relation, implying that they should operate very similar rotation-dependent dynamos in which the tachocline would not be a crucial ingredient. Landin et al. (2023) present a

theoretical and observational review of stellar magnetic activity in pre-MS and MS stars.

Low-mass stars in young clusters (ages ≤ 100 Myr) are known to be very active and to exhibit strong magnetic fields (specially those fast rotating), even though they do not follow the Skumanich law ($\Omega \propto t^{-2}$, Alphenaar & van Leeuwen 1981). For a few million years, their magnetic field lines are supposed to be anchored in a circumstellar disk, formed during the star formation process, within a few stellar radii. The interaction between the stellar magnetic field and the disk regulates the star's angular velocity, counteracting the tendency to spin up due to accretion of disk material of high specific angular momentum and to readjustments in the moment of inertia as the star contracts towards the MS. The magnetic torques acting on the central star during the disk lifetime transfer large amounts of its angular momentum to the disk and impose the star to rotate with a virtually constant surface angular velocity.

The observed rotation rates of stars in clusters of different ages suggest that the fast rotation phenomenon depends on mass. According to several works, such as those of Stauffer et al. (1997), Prosser et al. (1995) and Stauffer & Hartmann (1987), rapid rotation decreases slower for lower mass stars (the spin-down time scales expected for stars with $M < 0.5 M_\odot$ are longer than those for stars with $M > 1.0 M_\odot$). Attridge & Herbst (1992) and Choi & Herbst (1996) showed that T Tauri stars in the Orion Nebula Cluster have a very characteristic rotation period distribution: Classical T Tauri stars (CTTS), which still accrete from a disk, have a narrow period distribution with a peak at about 8-10 days, while Weak-line T Tauri stars (WTTS), that no longer accrete from a disk, have a broader distribution showing only a tail of slow rotators. In addition, WTTS appear to rotate faster, on average, than CTTS (Henderson & Stassun 2012). Orion Nebula Cluster (ONC, 1 Myr), NGC 2264 (3.5 Myr), IC 348 (2.5 Myr) and NGC 2362 (3.3 Myr) are some of the most studied young stellar clusters and all of them exhibit bimodal and dichotomic rotation period distributions. The bimodality is related to the presence of two peaks in the period distribution and the dichotomy is associated to the mass dependence of the distribution. Detailed studies of the rotation history of these clusters can be found in the literature, for example: ONC was analysed by Herbst et al. (2002), NGC 2264 was investigated by Lamm et al. (2005), Cieza & Baliber (2006) studied IC 348, Irwin et al. (2008) examined NGC 2362, the rotational properties of ONC and NGC 2264 was reviewed by Landin et al. (2016) and Landin et al. (2021) inspected such properties of IC 348 and NGC 2362. As the distribution of rotation periods in the pre-MS must evolve towards that of the MS, we have to be able to describe the process that leads from the wide distribution seen in the pre-MS to the even wider one seen in the MS. However, there is not a single model that manages to do this. In order to reproduce the evolution of stars that reach the MS with the highest rotation rates (near their breakup velocities), one should consider an evolution conserving angular momentum during all the pre-MS phase. On the other hand, to yield the rotation of stars spinning with a small fraction of their breakup velocities, one should consider that these stars were locked to their disks for a given time, keeping their angular velocities constant, and only after the locking phase they were released to spin up conserving angular momentum. Landin et al. (2016) present a theoretical and observational review of angular momentum evolution of pre-main sequence stars.

In this work, we use the ATON stellar evolution code to investigate the influence of the disk-locking mechanism on local convective turnover times and, consequently, on the Rossby num-

bers, and in the rotation-magnetic activity relation itself. Observational data of rotation periods, fractional X-ray luminosities and unsigned average large-scale surface magnetic fields from Vidotto et al. (2014) are used to constrain our models.

In Section 2, we briefly describe the ATON code and the input parameters used in this work. Section 3 presents and discusses our results on convective turnover times and convective velocities obtained with disk-locking and angular momentum conserving models. Our new theoretical local convective turnover times are compared to those existing in the literature and observational data are used to test our theoretical results in Section 4. Finally, Section 5 presents our conclusions.

2. Models and input physics

In the ATON code version used in this work, convection is treated according to the traditional Mixing Length Theory (Böhm-Vitense 1958), with the parameter representing the convection efficiency set as $\alpha=2$. Surface boundary conditions were obtained from non-grey atmosphere models (Allard et al. 2000) with a match between surface and interior at an optical depth of 10. We used the opacities reported by Iglesias & Rogers (1993) and Alexander & Ferguson (1994) and the equations of state from Rogers et al. (1996) and Mihalas et al. (1988). We assume that the elements are mixed instantaneously in convective regions. Our tracks start from a fully convective configuration with central temperatures in the range $5.35 < \log_{10}(T_c/\text{K}) < 5.70$, follow deuterium and lithium burning, and end at the MS configuration, as discussed in Landin et al. (2006), who also presented a detailed discussion about the zero point ages of stellar models.

We generated two sets of models. In the first (hereafter AMC models), we considered conservation of angular momentum throughout all stellar evolution. In the second set (hereafter DL models), we simulated the disk-locking mechanism, by considering an evolution with constant angular velocity during the first evolutionary stages, followed by conservation of angular momentum. In these models, the star-disk interaction treatment is not included in the code, and its effects on the stellar rotation are only mimicked by locking it for a while (Landin et al. 2016).

For AMC models, the initial angular momentum of each model was obtained according to the Kawaler (1987) relation¹

$$J_{\text{kaw}} = (1.562 \pm 0.504) \times 10^{50} \left(\frac{M}{M_{\odot}} \right)^{(0.985 \pm 0.140)} \text{ g cm}^2 \text{ s}^{-1}. \quad (1)$$

These initial angular momenta correspond to periods of ~ 15 days for a $0.1 M_{\odot}$ model and ~ 418 days for a $1.2 M_{\odot}$ model.

For DL simulating models, the initial angular momentum corresponds to the locking period, P_{lock} , of $\sim 8 \text{ days}^2$ based on the period distribution of CTTS in the ONC presented by Herbst et al. (2002). To investigate the effect of using different locking periods on τ_c , we ran some additional DL models with $P_{\text{lock}}=400$ days. The disk lifetimes, T_{disk} , used in this work are 1 and 3 Myr, because according to Monsch et al. (2023), the majority of circumstellar disks dissipate after $\sim 1\text{-}3$ Myr.

¹ For $M \geq 0.2 M_{\odot}$, we used the central values given by the Kawaler (1987) relation to obtain the initial angular momentum (J_{in}) of our models. Due to non-convergence reasons, we used a slightly smaller value of J_{kaw} as J_{in} for $0.1 M_{\odot}$, namely $J_{\text{in}}=7.943 \times 10^{48} \text{ g cm}^2 \text{ s}^{-1}$, which corresponds to a rotation period of ~ 30 days and is within the error bars in Eq. 1.

² Also due to non-convergence reasons, we used initial angular momenta smaller than those corresponding to 8 days for models with $M \geq 0.8 M_{\odot}$. The values used correspond to rotation periods of 8.5, 9.6, 10.6, 11.4 and 18.8 days for 0.8, 0.9, 1.0, 1.1 and $1.2 M_{\odot}$, respectively.

The evolutionary tracks were computed in the mass range of 0.1 to $1.2 M_{\odot}$ (in $0.1 M_{\odot}$ steps). We adopt the solar chemical composition ($X=0.7155$ and $Z=0.0142$) by Asplund et al. (2009). More details on the physics of the ATON models are given by Landin et al. (2006, 2023).

The current version of the ATON code allows for choosing among three rotational schemes (Mendes et al. 1999), (1) rigid body rotation throughout the whole star, (2) local conservation of angular momentum in the whole star (which leads to differential rotation) and (3) local conservation of angular momentum in radiative regions plus rigid body rotation in convective regions. Internal redistribution of angular momentum and angular momentum loss by stellar magnetised winds are implemented in the ATON code only for rotational scheme 3. However, there is observational evidence that the Sun's radiative core rotates as a solid body and the convective envelope rotates differentially, opposite to scheme 3 (Thompson et al. 2003). Here, our rotating models were generated according to scheme 1, because this is the only rotational scheme for which disk-locking mechanism is implemented in the ATON code. We leave for the future the implementation of a 4th rotational scheme with a rotational profile closer to that of the Sun and disk-locking mechanism for all rotational schemes.

3. Theoretical results

By using the version of the ATON code described in Landin et al. (2023), we followed the evolution of local convective turnover times from the pre-MS to the beginning of the MS for $0.1\text{-}1.2 M_{\odot}$ stars and tabulated them together with the corresponding evolutionary tracks. Table 1 presents the $1 M_{\odot}$ DL model ($P_{\text{lock}} \sim 8$ days and $T_{\text{disk}} = 3$ Myr) as an example of such tables. For DL models, rotation periods start from the value given by the P_{lock} parameter, are kept constant during the first million years (according to the T_{disk} parameter) and then evolve considering conservation of angular momentum from this time on. For models considering angular momentum conservation during all stages of evolution, the initial rotation periods are obtained from the initial angular momenta given in Eq. 1.

The initial angular velocities of most of our DL models are higher than those of AMC models. However, the angular velocity, Ω , is kept constant during 3 Myr in the DL models, while in the AMC models the stars are free to spin up since the beginning of their evolutions. As a consequence, AMC models become faster than DL models in the first million years of evolution, reaching the ZAMS with higher angular velocities (for $1.0 M_{\odot}$, for example, $\Omega_{\text{AMC}} \approx 4 \Omega_{\text{DL}}$ at the ZAMS).

As can be seen in Table 1, our $1 M_{\odot}$ model at the solar age shows a rotation period of 1.389 days, which is quite different from the current Sun. This is mainly due to the fact that we did not take into account some physical phenomena such as angular momentum loss by stellar winds. Such phenomena have large impact on the rotation rate, which in turn has a secondary effect on local convective turnover times, that are mainly determined by the mass of the model. According to our $1 M_{\odot}$ DL model, at the age of the Sun, the solar local convective turnover time is $\tau_{c,\odot}=14.13$ days, which corresponds to $Ro_{\odot}=1.77$ by using $P_{\text{rot},\odot}=25$ days (the same value used by Vidotto et al. 2014). This value is consistent to that found semi-empirically by Pizzolato et al. (2003), which is $\tau_{c,\odot}=12.59$ days ($Ro_{\odot}=1.99$).

Table 1. Evolutionary track for $1 M_{\odot}$ star (DL model with $P_{\text{lock}} \sim 8$ days and $T_{\text{disk}} = 3 \text{ Myr}^a$).

$\log \frac{t}{\text{yr}}$	$\log \frac{L}{L_{\odot}}$	$\log (T_{\text{eff}}/\text{K})$	$\log (g/\text{cm s}^{-2})$	$\log (\tau_c/\text{d})$	$\log (\tau_g/\text{d})$	P_{rot}/d	Ro	M_{rad}/M_{\odot}
2.233	1.665	3.600	2.127	1.976	2.910	10.580	0.112	0.000
3.668	1.601	3.623	2.280	1.901	2.805	10.580	0.133	0.000
4.203	1.382	3.634	2.545	1.892	2.792	10.580	0.136	0.000
4.643	1.163	3.642	2.795	1.874	2.708	10.580	0.141	0.000
5.186	0.989	3.647	2.989	1.871	2.687	10.580	0.143	0.000
5.352	0.836	3.651	3.158	1.870	2.781	10.580	0.143	0.000
5.606	0.615	3.653	3.389	1.869	2.785	10.580	0.143	0.000
5.882	0.394	3.652	3.604	1.873	2.810	10.580	0.142	0.000
6.164	0.173	3.646	3.802	1.942	2.853	10.580	0.121	0.003
6.454	-0.048	3.637	3.987	2.144	2.589	10.580	0.076	0.160
6.779	-0.253	3.632	4.173	2.059	2.406	6.859	0.060	0.428
7.054	-0.316	3.650	4.305	1.893	2.211	4.469	0.057	0.680
7.248	-0.221	3.689	4.367	1.683	1.990	3.020	0.063	0.853
7.372	-0.049	3.734	4.376	1.439	1.756	2.082	0.076	0.946
7.478	0.019	3.766	4.437	1.177	1.504	1.418	0.094	0.983
8.563	-0.092	3.759	4.520	1.213	1.521	1.354	0.083	0.980
9.277	-0.043	3.764	4.487	1.187	1.500	1.363	0.089	0.982
9.490	-0.001	3.767	4.458	1.178	1.481	1.372	0.091	0.984
9.624	0.040	3.769	4.427	1.150	1.460	1.389	0.098	0.985
9.743	0.094	3.772	4.384	1.142	1.443	1.423	0.103	0.986

Notes. Column 1 gives the \log_{10} of stellar age; col. 2 the \log_{10} of bolometric luminosity; col. 3 the \log_{10} of effective temperature; col. 4 the \log_{10} of effective gravity; col. 5 the \log_{10} of local convective turnover time; col. 6 the \log_{10} of global convective turnover time; col. 7 the rotation period; col. 8 the Rossby number; and col. 9 the radiative core mass. Throughout this work all the logarithms are in base 10.

^(a) The complete version of the table, including 24 tracks for masses in the range $0.1\text{--}1.2 M_{\odot}$ (in $0.1 M_{\odot}$ increments) for DL and AMC models, is available at the CDS.

3.1. Convective velocities calculations

In the framework of the Mixing Length Theory, which provides a description of the average behaviour of convective motions, the convective velocity, v_c , of the rising or falling material is related to its excess or deficit of temperature. For a given stellar mass and age, v_c increases radially outwards in the star (see Fig. 6 of Landin et al. 2023), and its value of greatest interest for this work is that used in the calculation of τ_c . Fig. 1 shows plots of convective velocities, which will be used for this purpose, as a function of age, for masses in the range of $0.1\text{--}1.2 M_{\odot}$ with $0.1 M_{\odot}$ increments. The convective velocities shown in Fig. 1 were evaluated for τ_c calculation at the traditional location, at one-half of a mixing length above the base of the convective zone, for partially convective configurations, while for fully convective configurations, v_c was estimated at the alternative location determined by Landin et al. (2023).

Values of v_c decrease during early phases of the pre-MS, increase after the formation of the radiative core and remain nearly constant during the MS; the higher the stellar mass, the higher the convective velocity. In the initial part of the pre-MS ($3 \lesssim \log(t/\text{yr}) \lesssim 6$), v_c is slightly lower for models simulating DL than for AMC models, while during the MS, models simulating DL yield higher convective velocities. This change in the v_c behaviour happens around 1 Myr, when AMC models become faster rotators than DL models.

The v_c behaviour can be understood by means of an extension of the mass-lowering effect (Sackmann 1970), which states that rotating stars mimic non-rotating stars with smaller masses. Here, we are extending the mass-lowering effect to stars with different rotation rates, in which stars with higher rotation rates mimic non-rotating stars with even lower masses than stars with lower rotation rates do. The fractional mass of the radiative core of each stellar mass for AMC and DL models, shown in Fig. 2,

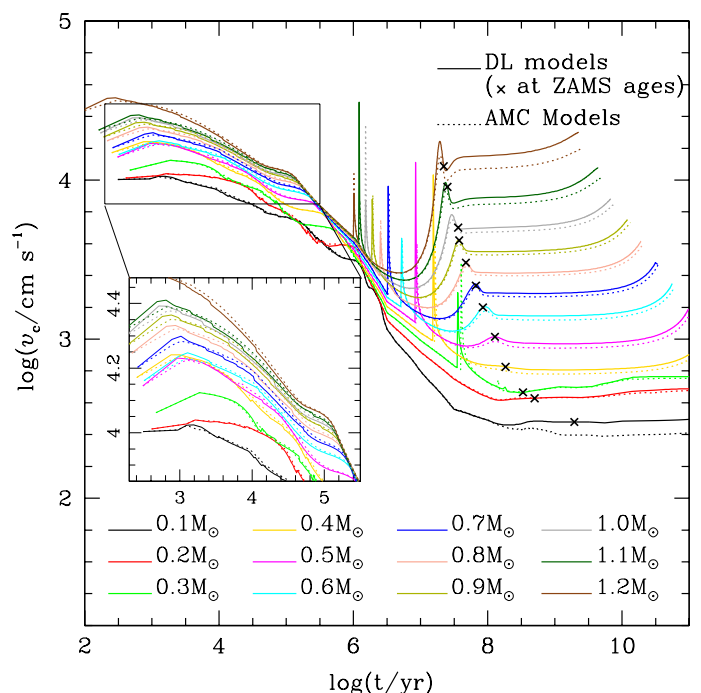


Fig. 1. Convective velocity as a function of age for different sets of models (DL models are drawn in solid lines and AMC models are shown in dotted lines). The curves referring to each stellar mass are drawn in a different colour according to the legend. Crosses (x) show the ZAMS ages for each mass model. The inset shows in detail the temporal evolution of v_c during the beginning of the pre-MS phase.

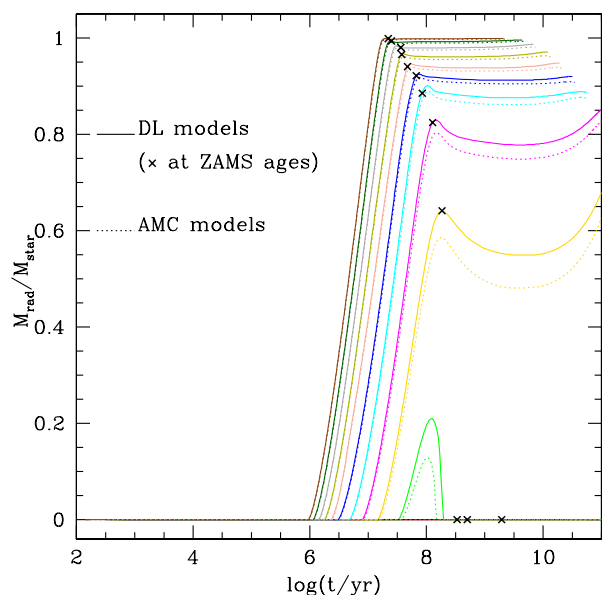


Fig. 2. Fractional mass of the radiative core for DL and AMC models. Symbols and colours are the same as in Fig. 1.

seem to corroborate our ideas. AMC models produce smaller fractional radiative core masses than DL models, as if they were models with smaller masses.

A consequence from the behaviour seen in Fig. 2 is that including disk-locking in the models results in weaker effects of rotation in the MS. During the disk-locking phase, stars contract keeping their angular velocities constant until the dissipation of

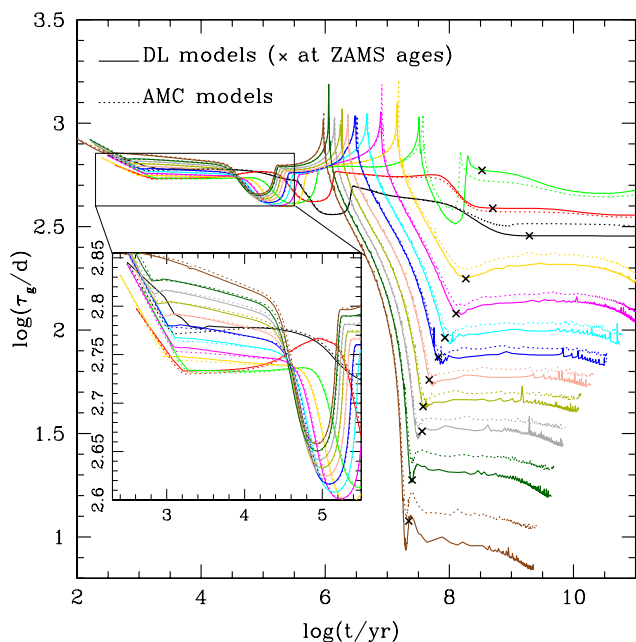


Fig. 3. Global convective turnover time as a function of age and stellar mass for different sets of models. The inset shows in detail the time evolution of τ_g during the beginning of the pre-MS phase. Colours and symbols are the same as in Fig. 1.

the disk (~ 3 Myr), when they start spinning-up conserving angular momentum, resulting in slower rotation rates in the MS, as compared with AMC models, that evolve without any locking. So, the faster the rotation, the stronger the mass-lowering effect and the slower the convective velocities.

In the MS the differences in v_c are higher for more massive stars, except for the $0.1 M_\odot$ model whose difference in convective velocity obtained by the two sets of models is comparable to that obtained by the $1.2 M_\odot$ model.

3.2. Global convective turnover times calculations

The global (or non-local) convective turnover time, τ_g , is defined as

$$\tau_g = \int_{R_b}^{R_{\text{star}}} v_c^{-1} dr, \quad (2)$$

where R_{star} is the stellar radius and R_b is the radial position of the base of the convective zone, the same as that of the tachocline for partially convective stars; $R_b=0$ (stellar centre) for fully convective stars. According to Kim & Demarque (1996), τ_g is the characteristic timescale of the convective overturn. It can be used to depict convection features of the whole stellar convective region at each evolutionary stage, representing an average convective timescale over the entire convective zone. In the absence of a suitable prescription to calculate local convective turnover times of fully convective stars, τ_g is used to evaluate their Rossby numbers instead of τ_c (Irving et al. 2023). Fig. 3 shows the global convective turnover times produced by AMC and DL models as a function of age and mass. The behaviour of τ_g is a consequence of its definition (Eq. 2), which depends directly on the actual extension of the convective zone (r_{conv}), but inversely on the convective velocity. For a star of a given mass and age, various combinations of these two effects can yield higher or lower τ_g , depending on which effect is dominant.

The behaviour of v_c was already discussed in Section 3.1 and before getting into the analysis of τ_g , we will describe the be-

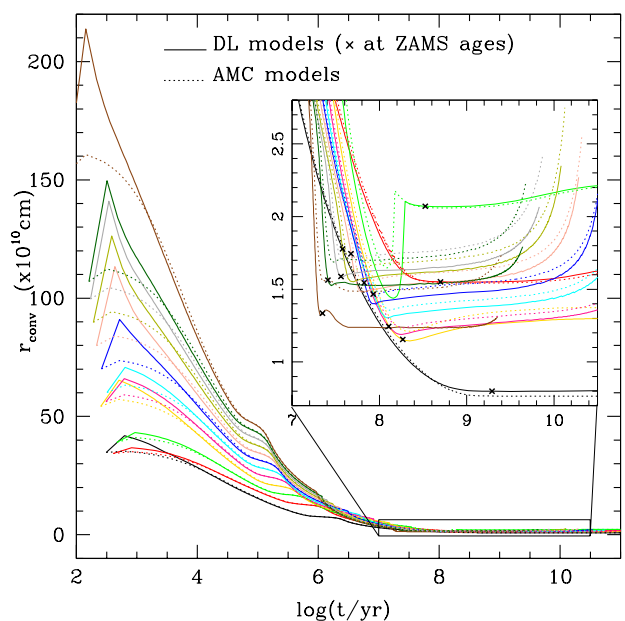


Fig. 4. Extension of the convective envelope in absolute terms (from the base to the top) as a function of mass and age for DL and AMC models. The inset shows in detail the time evolution of r_{conv} during the MS phase. Symbols and colours are the same as in Fig. 1.

haviour of the extension of the convective zone in absolute terms. Fig. 4 shows how r_{conv} varies with mass, age and model used. In the pre-MS (to the left of the crosses defining the ZAMS), r_{conv} increases with mass and decreases with the stellar age. In the very early phase of evolution (up to 10^3 to 10^4 years, depending on the stellar mass), r_{conv} produced by AMC models is smaller than that yielded by DL models. After that age (and up to the ZAMS), the behaviour of r_{conv} is reversed. In the MS (to the right of the crosses in Fig. 4), r_{conv} shows small changes with age for a given mass, but varies in a more complex way with mass. It sharply increases with mass from 0.1 to $0.3 M_\odot$, decreases abruptly from 0.3 to $0.4 M_\odot$ (because the star develops a radiative core), then gradually increases from 0.4 to $1.0 M_\odot$, reaches a local maximum (smaller than that for $0.3 M_\odot$), and decreases again from 1.0 to $1.2 M_\odot$. According to the model used, DL models produce r_{conv} larger than AMC models for MS stars with $M \leq 0.3 M_\odot$, while for MS stars with $M > 0.3 M_\odot$ AMC models yield larger r_{conv} than DL models do.

As well as Landin et al. (2023), we noticed that the time evolution of τ_g , showed in Fig. 3, is different for fully and partially convective stars. For very low-mass stars ($M \leq 0.3 M_\odot$), one can see only small variations (a factor of 3.5) on global convective turnover times, while variations reach almost 4 orders of magnitude for stars with $M > 0.3 M_\odot$.

For $M \leq 0.3 M_\odot$, the global convective turnover time does not vary significantly with age during the pre-MS and MS phases of evolution (less than an order of magnitude). In the beginning of the pre-MS ($t \leq 10^6$ years), τ_g decreases with increasing mass, but in the MS the opposite way of behaving is observed. This is due to the behaviour of v_c and r_{conv} (Figs. 1 and 4, respectively), which essentially increase with mass for all ages, so that the former contributes to decrease τ_g and the latter contributes to increase it. In the pre-MS, the dominant effect on τ_g is that of v_c and in the MS the dominant effect is that provided by r_{conv} .

For $M > 0.3 M_\odot$, τ_g values do not change significantly with age for a given mass in the beginning of the pre-MS phase, in

which stars are fully convective, then decrease when the radiative core is formed and remain roughly constant during the MS phase. In the pre-MS, the higher the stellar mass the higher τ_g . As can be seen in Figs. 1 and 4, both v_c and r_{conv} basically increase with mass for all ages, such that the effect of v_c leads to a decrease in τ_g , while r_{conv} causes an increase in τ_g . In this initial evolutionary phase, the influence of r_{conv} dominates that of v_c in the behaviour of τ_g . In the MS, τ_g increases with decreasing mass. Across this entire mass range, v_c increases with the stellar mass, contributing to decrease τ_g , while r_{conv} has a more complex behaviour. In the mass ranges $0.3\text{-}0.4M_\odot$ and $1.0\text{-}1.2M_\odot$, r_{conv} decreases with mass, reinforcing the effect of v_c and contributing to reduce τ_g with mass, and in the range $0.4\text{-}1.0M_\odot$, r_{conv} increases with mass, opposing the effect of v_c and contributing to increase τ_g with mass. The combination of these two effects results in the prevalence of v_c in the behaviour of τ_g , making τ_g decrease with increasing mass.

In our calculated models, the behaviour of τ_g depends on the stellar mass. In the beginning of the pre-MS, the global convective turnover time is practically model independent. For $M \geq 0.8M_\odot$, AMC models generate τ_g slightly longer than DL models, while for $M < 0.7M_\odot$, the opposite trend is observed. It seems that $0.7M_\odot$ is a transition mass for this behaviour. In the MS, τ_g is shorter for DL models in comparison with AMC ones ($\tau_{g,\text{DL}} < \tau_{g,\text{AMC}}$), except for 0.2 and $0.3M_\odot$. For $M \leq 0.3M_\odot$, DL models produce larger convective zones than AMC models ($r_{\text{conv,DL}} > r_{\text{conv,AMC}}$), favouring $\tau_{g,\text{DL}} > \tau_{g,\text{AMC}}$, while the convective velocities yielded by DL models are larger than those produced by AMC models ($v_{c,\text{DL}} > v_{c,\text{AMC}}$), favouring $\tau_{g,\text{DL}} < \tau_{g,\text{AMC}}$. The interplay between these two effects is dominated by the size of the convective zone for 0.2 and $0.3M_\odot$ (producing $\tau_{g,\text{DL}} > \tau_{g,\text{AMC}}$) and by the convective velocity for $0.1M_\odot$ (yielding $\tau_{g,\text{DL}} < \tau_{g,\text{AMC}}$). Among the fully convective models ($M \leq 0.3M_\odot$), one sees that the behaviour of DL and AMC models for $0.1M_\odot$ is the opposite of those of 0.2 and $0.3M_\odot$. This can be explained by the fact that v_c (Fig. 1) produced by AMC models for 0.2 and $0.3M_\odot$ are only slightly lower than those yielded by DL models while, for $0.1M_\odot$, AMC models produce v_c noticeably lower than DL models do. Analyses with finer mass grid models ($0.085, 0.09, 0.11, 0.12, 0.13, 0.14$ and $0.15M_\odot$, not shown here) reveal that such a switch in τ_g behaviour occurs between 0.10 and $0.11M_\odot$ and $\tau_{g,\text{DL}}$ continues smaller than $\tau_{g,\text{AMC}}$ for masses smaller than $0.10M_\odot$ (see the following quantitative comparisons between DL and AMC values of τ_g at 10 Gyr : $\tau_{g,\text{DL}}/\tau_{g,\text{AMC}}$ is 1.0251 for $0.2M_\odot$, 1.0041 for $0.11M_\odot$, 0.8765 for $0.10M_\odot$, 0.8423 for $0.09M_\odot$ and 0.9102 for $0.085M_\odot$). As the additional AMC models also present convergence issues when adopting the central values of J_{Kaw} as J_{in} , we used smaller input values which vary from $0.987 J_{\text{Kaw}}$ for $0.085M_\odot$ to $0.997 J_{\text{Kaw}}$ for $0.15M_\odot$. According to our AMC models, τ_g decreases with increasing J_{in} . If it were not for some convergence difficulties and had we used $J_{\text{in}} = J_{\text{Kaw}}$ for models with $M \leq 0.15M_\odot$, we would have obtained $\tau_{g,\text{DL}}$ even smaller than $\tau_{g,\text{AMC}}$, making the change in τ_g behaviour near $0.1M_\odot$ even more pronounced. For $M > 0.3M_\odot$, the behaviour of τ_g depending on the model used can be explained in a much simpler way, given that $r_{\text{conv,DL}} < r_{\text{conv,AMC}}$ and $v_{c,\text{DL}} > v_{c,\text{AMC}}$, both effects contribute to generate $\tau_{g,\text{DL}} < \tau_{g,\text{AMC}}$.

3.3. Local convective turnover times calculations

The characteristic convective overturn timescale used to compute Rossby numbers is the local convective turnover time, which differs from τ_g only by a factor. It is defined as $\tau_c = \ell/v_c$

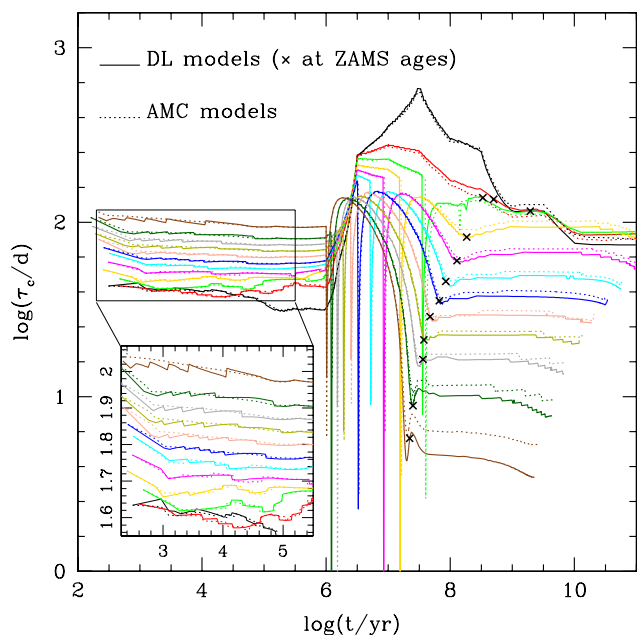


Fig. 5. Local convective turnover time as a function of age and stellar mass for different sets of models. Symbols and colours have the same meanings as in Fig. 1. The inset shows in detail the time evolution of τ_c during the beginning of the pre-MS phase.

and is evaluated in deep regions of the convective envelope, where dynamo generation of magnetic fields is supposed to take place (Kim & Demarque 1996). Fig. 5 shows local convective turnover times as a function of age and mass. For partially convective configurations, τ_c was calculated at the standard location, r , one-half of a mixing length above the base of the convective zone. For fully convective configurations (whose r are larger than the stellar radii), τ_c was calculated at an alternative place related to H_p , as described in Landin et al. (2023). τ_c behaves roughly as τ_g , both as a function of age and as a function of mass, with some differences in the low mass regime and in the range of $1\text{-}11\text{ Myr}$, when τ_c produced by models with $M \leq 0.3M_\odot$ become smaller than those for $0.4M_\odot$ models, as opposed to what happens regarding τ_g . This is probably due to the method used to calculate τ_c for fully convective stars, based on different linear fits for different age intervals and excluding higher masses because they deviate more from the linear behaviour; see Landin et al. (2023) for more details. In the pre-MS, τ_c is approximately constant and does not show a strong dependence with modelling (differences are around 1%). AMC models tend to produce higher τ_c for higher masses ($M > 0.7M_\odot$) and DL models tend to yield higher τ_c for smaller masses ($M < 0.6M_\odot$). As the stellar age increases, the cumulative effects of evolving with a higher angular velocity reflect in the convective properties of the stars and the differences in τ_c produced by the two sets of models reach $8\text{-}10\%$ for ages greater than 100 Myr . Stars with $M \geq 1M_\odot$ present the highest differences. In the MS, values of τ_c generated with models simulating the DL mechanism are shorter than those obtained with AMC models, except for 0.2 and $0.3M_\odot$, repeating the previously described behaviour of τ_g .

The top panel of Figure 6 shows the local convective turnover time as a function of age and mass produced by DL models with different locking periods ($P_{\text{lock}} \sim 8\text{ days}$ and $P_{\text{lock}} = 400\text{ days}$, keeping the same $T_{\text{disk}} = 3\text{ Myr}$). For clarity, we show plots only for 4 stellar mass models, $0.1, 0.4, 0.7$ and $1.0M_\odot$. DL models with longer locking periods produce slightly longer values of lo-

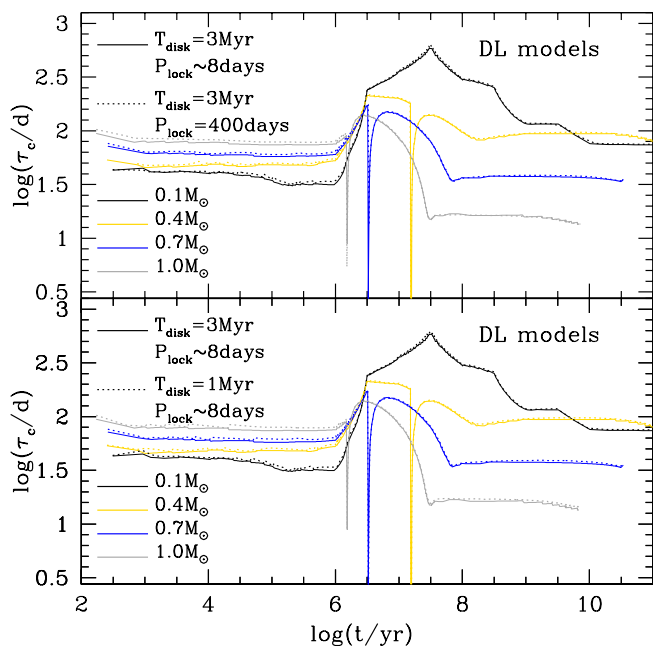


Fig. 6. Local convective turnover time as a function of age and mass for DL models with different locking periods (top panel) and different disk lifetimes (bottom panel). Colours are the same as in Fig. 1.

cal convective turnover times (except for the $1.0 M_{\odot}$ at the MS, for which τ_c is almost model independent). The reason is that DL models with $P_{\text{lock}}=400$ days have larger mixing lengths and convective velocities than those with $P_{\text{lock}}=8$ days, that contribute to increase and decrease τ_c , respectively, and the dependence on ℓ dominates over that on v_c . The bottom panel of Fig. 6 shows the local convective turnover time as a function of age and mass produced by DL models with different disk lifetimes ($T_{\text{disk}}=1$ and 3 Myr, keeping the same $P_{\text{lock}}\sim 8$ days). We again show plots only for 4 stellar mass models, 0.1 , 0.4 , 0.7 and $1.0 M_{\odot}$. For all evolutionary phases and masses, DL models with $T_{\text{disk}}=1$ Myr yielded slightly longer τ_c than DL models with $T_{\text{disk}}=3$ Myr, because, while ℓ is almost independent on T_{disk} , DL models with $T_{\text{disk}}=1$ Myr produce convective velocities slightly lower than those with $T_{\text{disk}}=3$ Myr, since $\tau_c \propto 1/v_c$.

τ_g and τ_c are quantities that cannot be directly observed and the best way to estimate them is through stellar evolutionary models. They are extensively used to determine Rossby numbers of stars operating different types of dynamos. τ_c is employed in stars that have tachocline-based dynamos and, when there is no suitable prescriptions to obtain it for stars that have no tachocline and harbour distributed dynamos, τ_g is used. τ_g and τ_c are mainly determined by the stellar mass, but non-standard physical ingredients, like the rotation rate, the way angular momentum evolves and disk-locking parameters, have secondary effects, as discussed in Sections 3.2 and 3.3.

After investigating the local convective turnover time behaviour as a function of age obtained by models with different DL parameters, Fig. 7 shows how τ_c and τ_g vary with the effective temperature at the ZAMS. This plot is of particular interest due to its adequacy in obtaining the Rossby number using a quantity obtainable through observational data. As both global and local convective turnover times practically do not change during the main sequence (see Figs. 3 and 5), their ZAMS values are representative for their entire main sequence. The effective

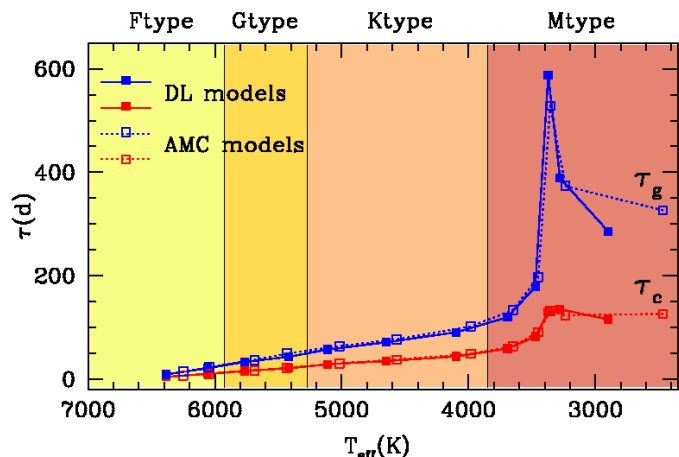


Fig. 7. Similarly to Fig. 13 of Irving et al. (2023), we show local (red) and global (blue) convective turnover times for AMC (dotted lines with open squares) and DL (solid lines with full squares) models as a function of effective temperature at the ZAMS. We used an updated version of Pecaut & Mamajek (2013) effective temperature-spectral type relation, https://www.pas.rochester.edu/emamajek/EEM_dwarf_UBVIJHK_colors_Teff.txt.

temperatures at the ZAMS, the ZAMS ages themselves, the global and local convective turnover times are slightly model dependent, and the differences increase with the decreasing effective temperatures (i.e. in the lower-mass regime).

4. Comparison with observations

In order to test our theoretical convective turnover times, we used them to calculate Ro for 73 late-F, G, K and M dwarf stars (both pre-MS and MS from the sample of Vidotto et al. 2014) and to investigate the magnetic activity-rotation relationship. The sample is formed by solar-like stars [MS stars with masses and ages in the ranges $0.66 \leq M/M_{\odot} \leq 1.34$ and $260 \leq t(\text{Myr}) \leq 8700$, including the Sun itself], young suns [non-accreting pre-MS and young MS stars with masses and ages in the ranges $0.54 \leq M/M_{\odot} \leq 1.50$ and $10 \leq t(\text{Myr}) \leq 130$], hot-Jupiter (h-J) hosts [MS stars with masses and ages in the ranges $0.79 \leq M/M_{\odot} \leq 1.34$ and $600 \leq t(\text{Myr}) \leq 5000$ that host planets as massive as Jupiter in very close orbits], M dwarfs [MS and non-accreting pre-MS stars with masses and ages in the ranges $0.10 \leq M/M_{\odot} \leq 0.75$ and $21 \leq t(\text{Myr}) \leq 1200$] and Classical T Tauri stars [accreting pre-MS stars with masses and ages in the ranges $0.65 \leq M/M_{\odot} \leq 2.00$ and $1.4 \leq t(\text{Myr}) \leq 17$]. Vidotto et al. (2014) separated their sample in these subsamples in order to investigate whether the stars in these subgroups showed any specific behaviour in the rotation-magnetic activity diagram. They did not find any particular trend for any of these subgroups other than those already known: fully convective stars tend to occupy the saturated region and partially convective ones occupy both regions. Values of mass, age (except for 12 M dwarfs and 1 T Tauri star), P_{rot} , L_X/L_{bol} and $\langle |B_V| \rangle$ were taken from Vidotto et al. (2014). The ages of the 12 M dwarfs without age estimates in Vidotto et al. (2014) were determined using our evolution models. The age of the T Tauri star CV Cha used by Vidotto et al. (2014) is 4.8 Myr, taken from the value of (5 ± 1) Myr determined by Hussain et al. (2009). By using this age and our local convective turnover time, the Rossby number of CV Cha is too high, diverging considerably from the typical values of other T Tauri stars of our sample (as can be seen as open green triangles in Figs. 8 and 9). We, then, took the inferior limit of the value published by Hussain et al. (2009), i.e. 4 Myr, as the age

of CV Cha, which coincides, within the errors, with the value of (4.2 ± 0.3) Myr found using the ATON code. Next, given the stellar mass and age of each object, their Rossby numbers were obtained using the observed rotation periods from Vidotto et al. (2014) and the local convective turnover times produced by our DL and AMC models. The rotation-activity relation of our sample was analysed using two different indicators of magnetic activity: L_X/L_{bol} and $\langle |B_V| \rangle$. Before getting into the details of our calculations, we outline the general procedure used for both indicators:

1. We initially fit the distribution of stars in the rotation-activity diagram with the following two-part, power-law functions,

$$\frac{L_X}{L_{\text{bol}}} = \begin{cases} C Ro^\beta, & \text{if } Ro > Ro_{\text{sat}}, \\ \left(\frac{L_X}{L_{\text{bol}}} \right)_{\text{sat}}, & \text{if } Ro \leq Ro_{\text{sat}}, \end{cases} \quad (3)$$

$$\langle |B_V| \rangle = \begin{cases} C Ro^\beta, & \text{if } Ro > Ro_{\text{sat}}, \\ \langle |B_V| \rangle_{\text{sat}}, & \text{if } Ro \leq Ro_{\text{sat}}, \end{cases} \quad (4)$$

where β is the power-law slope in a log-log plot for the unsaturated region and C is a constant. Given an initial guess value for Ro_{sat} , we determined either $(L_X/L_{\text{bol}})_{\text{sat}}$ or $\langle |B_V| \rangle_{\text{sat}}$, which are respectively the average values of L_X/L_{bol} and $\langle |B_V| \rangle$ for $Ro \leq Ro_{\text{sat}}$. For $Ro > Ro_{\text{sat}}$, we fit the data by using an iterative linear regression fit in a log-log scale, keeping the constant coefficient fixed, so that the values of either L_X/L_{bol} or $\langle |B_V| \rangle$ at Ro_{sat} are respectively equal to $(L_X/L_{\text{bol}})_{\text{sat}}$ and $\langle |B_V| \rangle_{\text{sat}}$.

2. Next we follow Vidotto et al. (2014) and Jackson & Jeffries (2010) and fixed the saturation Rossby number at its canonical value, $Ro_{\text{sat}}=0.1$, first estimated by Pizzolato et al. (2003), and determined the best parameters that fit the data to Eqs. 3 or 4, i.e. β and $(L_X/L_{\text{bol}})_{\text{sat}}$ or $\langle |B_V| \rangle_{\text{sat}}$. This approach will be referred to as ‘‘Method A’’.
3. A second estimate of Ro_{sat} is obtained by using an iterative least squares method to find the value at which the standard deviation of the data reaches its minimum and, again, we get the corresponding values of $(L_X/L_{\text{bol}})_{\text{sat}}$, $\langle |B_V| \rangle_{\text{sat}}$ and the best fitting slopes for the unsaturated region for both L_X/L_{bol} and $\langle |B_V| \rangle$ indicators. This approach will be referred to as ‘‘Method B’’.
4. A third and last estimate for Ro_{sat} is made by choosing the value for which a least squares fit to the data results in the best fit to the Sun at its maximum, average and/or minimum activity levels. Then, as previously, we obtain the corresponding values of $(L_X/L_{\text{bol}})_{\text{sat}}$, $\langle |B_V| \rangle_{\text{sat}}$ and β . This approach will be referred to as ‘‘Method C’’.

4.1. Using L_X/L_{bol} as the magnetic activity indicator

Among the 73 stars in the sample of Vidotto et al. (2014), 11 have no fractional X-ray luminosity determination, reducing our sample to 62 stars in the analysis involving L_X/L_{bol} as the magnetic activity indicator. We initially analysed the rotation-activity relationship of our sample by using L_X/L_{bol} and Ro calculated with τ_c from DL models with $P_{\text{lock}} \sim 8$ days and $T_{\text{disk}}=3$ Myr. The left panel of Fig. 8 shows our star sample in the $\log(L_X/L_{\text{bol}}) \times \log(Ro)$ plane, with different symbols and colours.

For $Ro_{\text{sat}}=0.1$ (Method A) the best fitting slope for the unsaturated part of the relation (see Eq. 3) was found to be $\beta = -1.9 \pm 0.2$, with the Pearson correlation coefficient $|\rho|=0.66$ and the saturation level was estimated to be $\log(L_X/L_{\text{bol}})_{\text{sat}} = -3.26 \pm 0.06$ (dotted curve in the left panel of Fig. 8). These values are consistent with those found by, e.g.

Table 2. Fit parameters of the rotation-magnetic activity relationship in this work, W11 (Wright et al. 2011), W18 (Wright et al. 2018) and G23 (Galvão et al. 2023).

Work	Ro_{sat}	β	$\log\left(\frac{L_X}{L_{\text{bol}}}\right)_{\text{sat}}$
DL mod., Meth. A	0.1	-1.9 ± 0.2	-3.26 ± 0.06
DL mod., Meth. B	0.042 ± 0.003	-1.3 ± 0.2	-3.20 ± 0.07
DL mod., Meth. C	0.19	-2.7 ± 0.4	-3.28 ± 0.05
AMC mod., Meth. A	0.1	-2.0 ± 0.2	-3.27 ± 0.06
AMC mod. Meth. B	0.049 ± 0.006	-1.5 ± 0.2	-3.20 ± 0.07
AMC mod., Meth. C	0.14	-2.4 ± 0.3	-3.28 ± 0.05
W11	0.13 ± 0.02	-2.7 ± 0.13	-3.13 ± 0.08
W18	$0.14^{+0.02}_{-0.04}$	$-2.3^{+0.4}_{-0.6}$	$-3.05^{+0.05}_{-0.06}$
G23	0.045 ± 0.001	-1.30 ± 0.08	-3.114 ± 0.006

Wright et al. (2011, 2018). For Ro_{sat} obtained through Method B, we found $Ro_{\text{sat}}=0.042 \pm 0.003$, $\beta=-1.3 \pm 0.2$ (with $|\rho|=0.80$) and $\log(L_X/L_{\text{bol}})_{\text{sat}}=-3.20 \pm 0.07$ (dashed curve in the left panel of Fig. 8). Although $\log(L_X/L_{\text{bol}})_{\text{sat}}$ obtained in the last case is consistent with those found in the literature, the values of β and Ro_{sat} are considerably higher and smaller, respectively. Notice that none of these methods fits the minimum or the maximum Sun (black circles). By applying Method C, we could not fit the minimum Sun, while the Sun’s position in its average level of activity (the average Sun) was only achieved with fitting parameters in disagreement with the literature. However, we could fit the maximum Sun and found $Ro_{\text{sat}}=0.19$, $\beta=-2.7 \pm 0.4$ (with $|\rho|=0.61$) and $\log(L_X/L_{\text{bol}})_{\text{sat}}=-3.28 \pm 0.05$ (solid black line in the left panel of Fig. 8).

These values are consistent with those found in the literature, with the value of β matching that of Wright et al. (2018) within the errors and coinciding with that of Wright et al. (2011). The value of Ro_{sat} is slightly larger than those of Wright et al. (2011, 2018) and $\log(L_X/L_{\text{bol}})_{\text{sat}}$ is moderately smaller than (but still consistent with) those obtained by both mentioned works. For these reasons, and also because this fit reproduces the maximum Sun’s position in the rotation-activity diagram with consistent parameters, we consider it the best fit using DL models. For comparison, the best fit found by Wright et al. (2011), obtained using another sample of stars, is also shown in the left panel of Fig. 8. Table 2 shows the fit parameters found in this subsection (using τ_c provided by DL models) and those found by Wright et al. (2011) and Wright et al. (2018).

Using values of τ_c calculated with AMC models, we obtained the Rossby number of all stars in our sample and displayed them in the rotation-activity diagram, as shown in the right panel of Fig. 8. As for the DL case, we fit the AMC data with three values of Ro_{sat} . For $Ro_{\text{sat}}=0.1$ (Method A) we found a power index $\beta=-2.0 \pm 0.2$ (with $\rho=0.69$) and a saturation level of $\log(L_X/L_{\text{bol}})_{\text{sat}}=-3.27 \pm 0.06$ (dotted curve in the right panel of Fig. 8). These values are consistent with those found in the literature, but $\log(L_X/L_{\text{bol}})_{\text{sat}}$ is slightly low. Then, by using Method B, we found $Ro_{\text{sat}}=0.049 \pm 0.006$, $\beta=-1.5 \pm 0.2$ (with $|\rho|=0.81$) and $\log(L_X/L_{\text{bol}})_{\text{sat}}=-3.20 \pm 0.07$ (dashed curve in the right panel of Fig. 8). These values of Ro_{sat} and β are compatible with those found in the literature, despite being marginally lower and higher, respectively, while the saturated value of L_X/L_{bol} matches the one found by Wright et al. (2011) within the uncertainties. Nearly identical parameters were obtained for this sample by Galvão et al. (2023), who used τ_c determined with

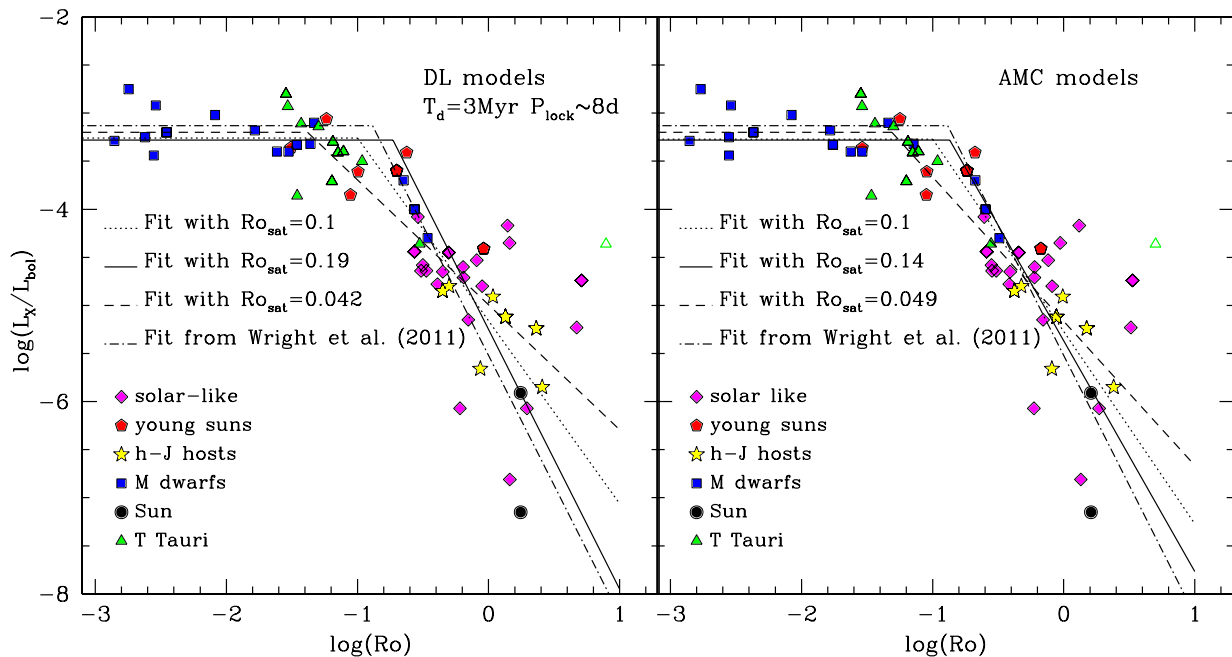


Fig. 8. $\log(L_X/L_{\text{bol}}) \times \log(Ro)$ for stars in the sample of Vidotto et al. (2014). In the left panel, τ_c values, which enter in Ro calculations, were obtained from DL models with $P_{\text{lock}} \sim 8$ days and $T_{\text{disk}} = 3$ Myr. In the right panel, τ_c values were obtained from AMC models. Solar-like stars are shown as \blacklozenge , the Sun in its maximum and minimum levels of activity as \bullet , young suns as \blacklozenge , hot-Jupiter hosts as \star , M dwarfs as \blacksquare and T Tauri stars as \blacktriangle .

evolutionary tracks from the ATON code (similar to AMC models) and a Markov Chain Monte Carlo (MCMC) fitting method. Again, as can be seen from the right panel of Fig. 8, the dotted and dashed curves do not fit the Sun. Using Method C, we obtained a saturation Rossby number of $Ro_{\text{sat}} = 0.14$. This method fits the maximum Sun, provides $\log(L_X/L_{\text{bol}})_{\text{sat}} = -3.28 \pm 0.05$ and $\beta = -2.4 \pm 0.3$ (with $|\rho| = 0.66$) and is shown as a solid curve in the right panel of Fig. 8. The value of Ro_{sat} agrees with those found by Wright et al. (2011) and Wright et al. (2018) and is moderately larger than that found by Landin et al. (2023), while the value of β agrees, within the uncertainties, with those found by Wright et al. (2011), Wright et al. (2018) and Landin et al. (2023), that used much larger samples of stars (824 stars for the former work and 847 stars for the latter ones). Likewise, this value of $\log(L_X/L_{\text{bol}})_{\text{sat}}$ is consistent with those found by these authors, although a little smaller. As in the case of DL models, this method cannot fit the minimum Sun and fits the average Sun with conflicting parameters. For the same reasons discussed in the analysis of the rotation-activity diagram with τ_c obtained by DL models, the parameters that fit the maximum Sun seem to be the more reliable ones when AMC models are used to calculate τ_c and they are shown in Table 2, together with the other AMC fits obtained in this subsection. For comparison purposes, the best fit found by Wright et al. (2011) using another sample of stars is also shown in the right panel of Fig. 8.

The values obtained for β and $\log(L_X/L_{\text{bol}})_{\text{sat}}$ with τ_c calculated by AMC models agree, within the errors, with the corresponding values obtained by DL models. Regarding the fits obtained with Methods A and B, the β values are slightly smaller for AMC models and the opposite situation is observed by the fits which reproduce the Sun’s position in its maximum activity level (Method C). For both sets of models, we consider that the fits which better predict the solar magnetic activity level are the best ones. Besides fitting the Sun, they present Ro_{sat} and β in

accordance with what was found in the works of Wright et al. (2011, 2018).

As we can see in Fig. 5, τ_c produced by AMC models are higher than those generated by DL models for most stellar ages, implying in smaller Rossby numbers. In fact, the average value of Rossby numbers obtained with DL models, $\langle Ro_{\text{DL}} \rangle$, is 21% higher than that obtained with AMC models, $\langle Ro_{\text{AMC}} \rangle$, which causes a slight global shift of the star distribution to the left in the rotation-activity diagram. However, this does not translate into a lower saturation Rossby number in our least squares fit, due to the high dispersion of the data. The fact that $\langle Ro_{\text{DL}} \rangle$ is larger than $\langle Ro_{\text{AMC}} \rangle$ indicates that stars that had experienced (or are experiencing) a locking phase present higher Rossby numbers and then, lower dynamo numbers, which means lower efficiency in the dynamo generation process.

It is already known that internal redistribution of angular momentum and angular momentum loss by stellar magnetised winds can significantly affect the stellar angular momentum evolution. As for the moment, we cannot consider yet these effects in our results because the ATON code version that takes the disk-locking mechanism into account is currently implemented only for rotational scheme 1 (solid body rotation), while the effects related to angular momentum variation are implemented only for rotational scheme 3 (differential rotation in radiative regions and solid body rotation in convective zones). At 100 Myr, τ_c obtained for 0.4 and 1.0 M_{\odot} models considering redistribution of angular momentum and angular momentum loss by winds is around 94% of the value obtained when considering solid body rotation with no effects related to angular momentum variability. As far as we could foresee, our DL and AMC models would be affected roughly the same way by the inclusion of such effects, keeping invariable the relative differences between our results obtained with the two sets of models. Including these effects would cause DL and AMC models to produce τ_c values a few percent lower.

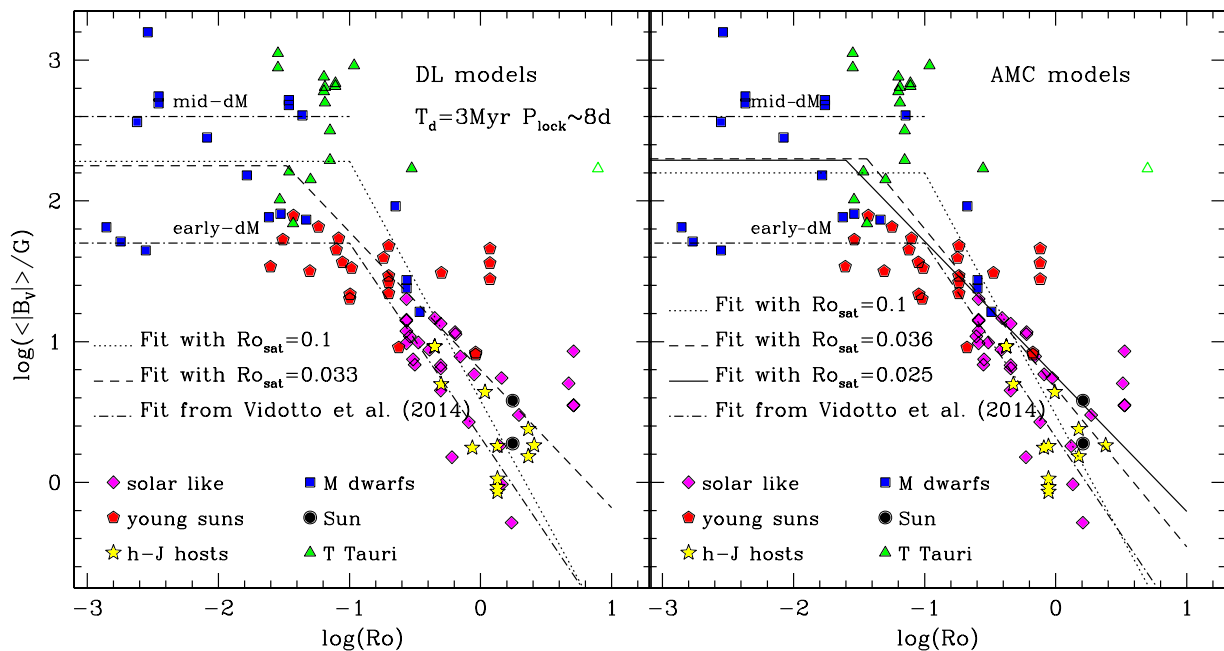


Fig. 9. $\log(\langle |B_V| \rangle) \times \log(Ro)$ for stars in the sample of Vidotto et al. (2014). In the left panel, the τ_c values, which enter in Ro calculations, were obtained from DL models with $P_{\text{lock}} \sim 8$ days and $T_{\text{disk}} = 3$ Myr. In the right panel, τ_c values were obtained from AMC models. Symbols are the same as in Fig. 8.

Consequently, the Rossby numbers obtained for the stars of our sample would be slightly higher (shifting the star distributions in both panels of Fig. 8 to the right), which would probably slightly increase Ro_{sat} . Nevertheless, we plan to improve the ATON code in order to fully account for these effects.

4.2. Using $\langle |B_V| \rangle$ as the magnetic activity indicator

The sample of Vidotto et al. (2014) consists of 104 magnetic maps of 73 stars, constructed with observations made at multiple epochs, resulting in 102 pairs of measurements of unsigned average large-scale surface magnetic fields and rotation periods, which allow us to use $\langle |B_V| \rangle$ as the magnetic activity indicator in the analysis of the rotation-activity relation of our sample. Initially, we used Rossby numbers calculated by DL models with $P_{\text{lock}} \sim 8$ days and $T_{\text{disk}} = 3$ Myr. In the left panel of Fig. 9, we show the stars of our sample in the $\log(\langle |B_V| \rangle) \times \log(Ro)$ plane with the same symbols and colours used in Fig. 8.

The same general procedure used for the $\log(L_X/L_{\text{bol}})$ indicator was adopted and, for $Ro_{\text{sat}} = 0.1$ (Method A), we found $\beta = -1.70 \pm 0.15$, as the best fitting slope for the unsaturated part of the relation (see Eq. 4), with $\rho = 0.66$, and the saturation level of activity was found to be $\log(\langle |B_V| \rangle / G)_{\text{sat}} = 2.28 \pm 0.06$ (dotted curve in the left panel of Fig. 9). The value of β is nearly in agreement with that of Vidotto et al. (2014) within the uncertainties. Our value of $\log(\langle |B_V| \rangle / G)_{\text{sat}}$ is between the saturation value found by Vidotto et al. (2014) for the early M dwarfs (early-dM, $M \geq 0.4 M_{\odot}$, $\log(\langle |B_V| \rangle / G)_{\text{sat}} = 1.7$) and the value found for mid M dwarfs (mid-dM, $0.2 < M / M_{\odot} < 0.4$, $\log(\langle |B_V| \rangle / G)_{\text{sat}} = 2.6$). These two saturation levels are shown as horizontal dot-dashed lines in both panels of Fig. 9. With Method B, we found $Ro_{\text{sat}} = 0.033 \pm 0.012$, $\beta = -0.98 \pm 0.11$ (with $|\rho| = 0.81$) and $\log(\langle |B_V| \rangle / G)_{\text{sat}} = 2.25 \pm 0.14$ (dashed curve in the left panel of Fig. 9). These values of β and $\langle |B_V| \rangle_{\text{sat}}$ are consistent with those found by Vidotto et al. (2014), but our β is slightly higher and

our Ro_{sat} is considerably lower. According to See et al. (2019), who also found a Ro_{sat} smaller than Vidotto et al. (2014) but a little larger than this work, obtaining a smaller value of Ro_{sat} could be due to a number of reasons. They mentioned that a poorly constrained level of the saturation field strength and differences in the way to calculate the convective turnover times can affect the Ro_{sat} value. In addition, they emphasise that different activity indicators could saturate at different Rossby numbers. As can be seen in the left panel of Fig. 9, our fit obtained through Method B fits the Sun in its maximum level of activity, while our fit with $Ro_{\text{sat}} = 0.1$ (Method A) nearly fits the Sun in its minimum. Although Method B fitted the maximum Sun, we applied Method C and, with it, we were also able to reproduce the minimum and the average Sun, in addition to the maximum Sun, with plausible parameters, similar to those found by See et al. (2019) and Galvão et al. (2023). We decided to present only the parameters that fit the maximum Sun because this was the only level of solar activity that we were able to reproduce with Method C, employing the two magnetic activity indicators used in this work. For comparison, the best fit found by Vidotto et al. (2014) is also shown in the left panel of Fig. 9 as dot-dashed lines. Here, it is worth mentioning that our fit includes all T Tauri stars and the 12 M dwarfs without age estimates in Vidotto et al. (2014) but these stars did not enter in their fit. Table 3 shows the fit parameters found in this subsection (using τ_c provided by DL models) and those found by Vidotto et al. (2014) and See et al. (2019).

Finally, we investigated the rotation-activity relationship of our sample by using our local convective turnover times obtained with AMC models to calculate the Rossby number of all stars. Our sample is displayed in the rotation-activity diagram shown in the right panel of Fig. 9 and the data were fit with the two-part power-law function expressed in Eq. 4. We again performed three fits to our data by imposing $\langle |B_V| \rangle = \langle |B_V| \rangle_{\text{sat}}$ at Ro_{sat} . For $Ro_{\text{sat}} = 0.1$ (Method A), we found $\beta = -1.72 \pm 0.15$ (with $\rho = 0.68$) and $\log(\langle |B_V| \rangle / G)_{\text{sat}} = 2.20 \pm 0.09$ (dotted curve in the right panel

Table 3. Fit parameters of the rotation-magnetic activity relation in this work, Vidotto et al. (2014), See et al. (2019) and Galvão et al. (2023).

Work	Ro_{sat}	β	$\log\left(\frac{\langle B_V \rangle}{G}\right)_{\text{sat}}$
DL mod., Meth. A	0.1	-1.70 ± 0.15	2.28 ± 0.06
DL mod., Meth. B	0.033 ± 0.012	-0.98 ± 0.11	2.25 ± 0.14
AMC mod., Meth. A	0.1	-1.72 ± 0.15	2.20 ± 0.09
AMC mod., Meth. B	0.036 ± 0.008	-1.13 ± 0.11	2.30 ± 0.12
AMC mod., Meth. C	0.25	-0.96 ± 0.10	2.29 ± 0.15
Vidotto et al. (2014)	0.1	-1.38 ± 0.14	1.7 (early-dM) 2.6 (mid-dM)
See et al. (2019)	0.06 ± 0.01	-1.40 ± 0.10	2.41 ± 0.12
Galvão et al. (2023)	0.059 ± 0.002	-1.23 ± 0.01	2.19 ± 0.01

of Fig. 9). This value of $\langle|B_V|\rangle_{\text{sat}}$ is between the values proposed by Vidotto et al. (2014) and in agreement with that of See et al. (2019) within the uncertainties and this value of β is consistent with that published by both works. Next, we applied Method B and found $Ro_{\text{sat}}=0.036 \pm 0.08$, $\beta=-1.13 \pm 0.11$ (with $\rho=0.80$) and $\log(\langle|B_V|\rangle/G)_{\text{sat}}=2.30 \pm 0.12$ (dashed curve in the right panel of Fig. 9). Although this Ro_{sat} is considerably smaller than others found in the literature (except that of See et al. 2019), this value of β matches that of Vidotto et al. (2014) within the errors and nearly matches that of See et al. (2019), and the value of $\langle|B_V|\rangle_{\text{sat}}$ is consistent with those found by both works. Even by using a different fitting method (MCMC), Galvão et al. (2023) also found similar parameters as in our analysis. As one can see in the right panel of Fig. 9, the dotted curve nearly fits the minimum Sun and the dashed curve is close to the maximum Sun. So, our last fit aimed to get a better fit to the maximum Sun by means of Method C, resulting in $Ro_{\text{sat}}=0.025$, which is considerably lower than the values found in the literature. This last fit also provides $\beta=-0.96 \pm 0.10$ and $\log(\langle|B_V|\rangle/G)_{\text{sat}}=2.29 \pm 0.15$ (with $|\rho|=0.81$, seen in solid line in the right panel of Fig. 9). These values are consistent with those found by Vidotto et al. (2014) and See et al. (2019), although the value of β is somewhat higher. With Method C, we could also fit both the minimum and the average Sun with consistent parameters. As in the previous analysis, the parameters that fit the Sun in the study of the rotation-activity relation using $\langle|B_V|\rangle$ as an activity indicator and τ_c generated by AMC models (all shown in Table 3) are also considered the more reasonable ones. For comparison, the best fit found by Vidotto et al. (2014) is also shown in the right panel of Fig. 9 as dot-dashed lines.

The values obtained for β and $\langle|B_V|\rangle_{\text{sat}}$ with τ_c calculated by AMC models agree, within the errors, with those obtained by the corresponding fits with τ_c calculated by DL models.

As described in Subsection 4.1, the values of Rossby numbers obtained with τ_c produced by AMC models are lower than those generated by DL models and this manifests itself as a slight shift of the stars distribution to the left in the right panel of Fig. 9 relative to those in the same figure's left panel. For this subsample, $\langle Ro_{\text{DL}} \rangle = 1.27 \langle Ro_{\text{AMC}} \rangle$, what would again imply that stars which pass through a locking phase would have a smaller dynamo number and, consequently would operate a less efficient dynamo. However, as in Subsection 4.1, $Ro_{\text{sat,DL}} < Ro_{\text{sat,AMC}}$, probably due to the high dispersion of the data. Lastly, the inclusion of redistribution of angular momentum and angular momentum loss by winds would affect the results obtained with DL and AMC models in a similar fashion, slightly increasing the

stars Rossby numbers and moving the whole star distributions in both panels of Fig. 9 to the right, as discussed in the previous subsection.

5. Conclusions

We present new sets of pre-MS and MS evolutionary tracks considering the disk-locking mechanism and the conservation of angular momentum, including Rossby numbers, global and local convective turnover times in the mass range of $0.1-1.2 M_{\odot}$. We compared τ_g , τ_c and v_c produced by the two sets of models considering both evolutionary phases (pre-MS and MS). The differences are smaller in the early pre-MS ($\sim 1\%$) and increase with stellar age, reaching 8-10% for ages greater than 100 Myr. The largest differences are found in stars with masses higher than or equal to $1 M_{\odot}$.

In the MS, models simulating the DL mechanism produce v_c higher than models conserving angular momentum. The opposite behaviour is observed for τ_g and τ_c , except for 0.2 and $0.3 M_{\odot}$ models. More specifically, our results point out that stars which experience a locking phase reach the MS with smaller values of τ_c , larger Rossby numbers and smaller dynamo numbers, implying that their dynamo processes are less efficient in comparison with those stars that evolve conserving angular momentum since the beginning. By varying the initial angular momentum and the duration of the disk phase, we noticed that the higher the initial velocity and T_{disk} , the shorter τ_c . As the local convective turnover time is used to obtain the Rossby number, this suggests that properties of the disk phase of the star affect its Ro and its position in the rotation-activity diagram in the MS.

In the sequence, we used our theoretical convective turnover times to calculate Ro for 73 stars from the sample of Vidotto et al. (2014) to investigate the magnetic activity-rotation relationship. We plot the data in two versions of the rotation-activity diagram ($L_X/L_{\text{bol}} \times Ro$ and $\langle|B_V|\rangle \times Ro$) which show the typical saturated and unsaturated regimes. We fit the data with two-part power-law functions (Eqs. 3 and 4) using three different methods. By considering the fit in the $L_X/L_{\text{bol}} \times Ro$ diagram (with τ_c calculated by DL models) which reproduces the active Sun's position (Method C), we found $Ro_{\text{sat}}=0.14$, $\log(L_X/L_{\text{bol}})_{\text{sat}}=-3.28 \pm 0.05$ and the inclination of the unsaturated region was found to be $\beta=-2.4 \pm 0.3$. By considering the best fit in the $\langle|B_V|\rangle \times Ro$ diagram which reproduces the Sun's position in its maximum of activity (obtained with Method B), we found $Ro_{\text{sat}}=0.033 \pm 0.012$, $\log(\langle|B_V|\rangle/G)_{\text{sat}}=2.25 \pm 0.15$ and the power index of the unsaturated region was found to be $\beta=-0.98 \pm 0.11$. These parameters are consistent to those usually found in the literature. We caution that these results are based on a relatively small sample, specially when it is compared to other similar works (for instance, Wright et al. 2011, 2018 and Newton et al. 2017). In addition, τ_c in Subsections 4.1 and 4.2 were obtained assuming either that all stars had gone through a disk phase (with about the same locking period and during the same disk lifetime) or that they all evolved conserving angular momentum from the beginning. The most likely scenario is that some stars would have evolved with a very short disk-locking phase ($T_{\text{disk}} \leq 10^5$ yr) and can be considered as having evolved without a circumstellar disk since the start of their evolutions, while others would have spent some time in a locking phase with different locking periods and different disk lifetimes.

Finally, we speculated how internal redistribution of angular momentum and angular momentum loss by magnetised stellar winds would affect our results. We took such effects into account in 0.4 and $1.0 M_{\odot}$ models which rotate according to rotational

scheme 3 and conserve angular momentum during all evolutionary phases and showed that it reduces τ_c in 6% at 100 Myr. We found no reason why these effects would affect DL models differently than AMC models (remembering that both were modelled with rigid body rotation). Therefore, the general behaviour we would expect for the stars in our sample in Section 4 is that they would have smaller τ_c , which would imply in a larger Ro and in a less efficient dynamo ($N_D \propto Ro^{-2}$).

Data Availability

The complete version of Table 1 is only available in electronic form at the CDS via anonymous ftp to cdsarc.u-strasbg.fr (130.79.128.5) or via <http://cdsweb.u-strasbg.fr/cgi-bin/qcat?J/A+A/>.

Acknowledgements. The authors thank Drs. Francesca D’Antona (INAF-OAR, Italy) and Italo Mazzitelli (in memoriam) for granting them full access to the ATON evolutionary code. They are also grateful to an anonymous referee for his/her many comments and suggestions that helped to improve this work. Financial support from the Brazilian agencies CAPES, CNPq and FAPEMIG is gratefully acknowledged.

References

- Alexander, D.R., Ferguson, J.W., 1994, *ApJ*, 437, 879
Allard, F., Hauschildt, P.H., Schweitzer, A., 2000, *ApJ*, 539, 366
Alphenaar, P., van Leeuwen, F., 1981, *Inf. Bull. Variable Stars*, No. 1957
Asplund, M., Grevesse, N., Sauval, A. J., Scott, P., 2009, *ARA&A*, 47, 481A
Attridge, J.M., Herbst, W., 1992, *ApJ*, 398, 61
Böhm-Vitense, E. 1958, *Z. Astroph.*, 46, 108
Cieza, L., Baliber, N., 2006, *ApJ*, 649, 862.
Choi, P.I., Herbst, W., 1996, *AJ*, 111, 283
Donati, J.-F., Landstreet, J.D., 2009, *ARA&A*, 47, 333
Durney, B.R., De Young, D.S., Roxburgh, I.W., 1993, *Sol. Phys.*, 145, 207
Flaccomio, E., Micela, G., Sciortino, S., 2003, *A&A*, 402, 277
Galvão, L.J., Landin, N.R., Alencar, S.H.P., 023, *Boletim da Sociedade Astronômica Brasileira*, 34, 157
Henderson, C.B., Stassun, K.G., 2012, *ApJ*, 747, 51
Herbst, W., Bailer-Jones, C.A.L., Mundt, R., Meisenheimer, K., Wackermann, R., 2002, *A&A*, 396, 513
Hussain, G.A.J., Collier Cameron, A., Jardine, M.M., Dunstone, N., Ramirez Velez, J., Stempels, H.C., Donati, J.-F., Semel, M., Aulanier, G., Harries, T., Bouvier, J., Dougados, C., Ferreira, J., Carter, B.D., Lawson, W.A., 2009, *MNRAS*, 398, 189.
Iglesias, C.A., Rogers, F.J., 1993, *ApJ*, 412, 752
Irving, A.Z., Saar, H.S., Wargelin, B.J., do Nascimento, J.D., 2023, *ApJ*, 949, 51
Irwin, J., Hodgkin, S., Aigrain, S., Bouvier, J., Hebb, L., Irwin, M., Moraux, E., 2008, *MNRAS*, 384, 675.
Jackson, R.J., Jeffries, R.D., 2010, *MNRAS*, 407, 465
Kawaler, S.D., 1987, *PASP*, 99, 1322
Kim, Y.-C., Demarque, P.S., 1996, *ApJ*, 457, 340
Lamm, M.H., Mundt, R., Bailer-Jones, C.A.L., Herbst, W., 2005, *A&A*, 430, 1005
Landin, N.R., Ventura, P., D’Antona, F., Mendes, L.T.S., Vaz, L.P.R., 2006, *A&A*, 456, 269
Landin, N.R., Mendes, L.T.S., Vaz, L.P.R., 2010, *A&A*, 510, 46
Landin, N.R., Mendes, L.T.S., Vaz, L.P.R., Alencar, S.H.P., 2016, *A&A*, 586, A96
Landin, N.R., Chaves, J.K.L., Souza, T.S.M., Mendes, L.T.S., Vaz, L.P.R., Alencar, S.H.P., 2021, *The 20.5th Cambridge Workshop on Cool Stars, Stellar Systems, and the Sun (CS20.5)*, online at <http://coolstars20.cfa.harvard.edu/cs20half>, id.329
Landin, N.R., Mendes, L.T.S., Vaz, L.P.R., Alencar, S.H.P., 2023, *MNRAS*, 519, 5304
Mendes, L.T.S., D’Antona, F., Mazzitelli, I., 1999, *A&A*, 341, 174
Mihalas, D., Dappen, W., & Hummer, D.G. 1988, *ApJ*, 331, 815
Mohanty, S., Basri, G., 2003, *AJ*, 583, 451
Monsch, K., Drake, J.J., Garraffo, C., Picogna, G., Ercolano, B., 2023, *ApJ*, 959, 140
Nelson, O.R., 2008, Ph.D. Thesis, Federal University of Rio Grande do Norte, Natal, Brazil
Newton, E.R., Irwin, J., Charbonneau, D., Berlind, P., Calkins, M.L., and Mink, J., 2017, *ApJ*, 834, 85
Noyes, R.W., Hartmann, S.W., Baliunas, S., Duncan, D.K., Vaughan A., 1984, *ApJ*, 279, 763
Parker, E.N., 1955, *ApJ*, 122, 293
Pecaut, M.J., Mamajek, E.E., 2013, *ApJS*, 208, 9P
Pizzolato, N., Maggio, A., Micela, G., Sciortino, S., and Ventura, P., 2003, *A&A*, 397, 147
Preibisch, T., Kim, Y.C., Favata, F., Feigelson, E.D., Flaccomio, E., Getman, K., Micela, G., Sciortino, S., Stassun, K., Stelzer, B., and Zinnecker, H., 2005, *ApJ*, 160, 401
Prosser C.F., Shetrone, M.D., Dasgupta, A., Backman, D.E., Laaksonen, B.D., Baker, S.W., Marschall, L.A., Whitney, B.A., Kuijken, K., Stauffer, J.R., 1995, *PASP*, 107, 211
Rogers, F.J., Swenson, F.J., & Iglesias, C.A. 1996, *ApJ*, 456, 902
Sackmann, I.-J., 1970, *A&A*, 8, 76
See, V., Matt, S.P., Folsom, C.P., Saikia, S.B., Donati, J.-F., Fares, R., Finley, A.J., Hébrard, E.M., Jardine, M.M., Jeffers, S.V., Lehmann, L.T., Marsden, S.C., Mengel, M.W., Morin, J., Petit, P., Vidotto, A.A., and Waite, I.A., 2019, *ApJ*, 876, 118
Spiegel, E.A., Zahn, J.-P., 1992, *A&A*, 265, 106
Stauffer, J.R., Hartmann, L.W., 1987, *ApJ*, 318, 337
Stauffer, J.R., Hartmann, L.W., Prosser, C.F., Randich, S., Balachandran, S., Paten, B.M., Simon, T., Giampapa, M., 1997b, *ApJ*, 479, 776
Skumanich, A., 1972, *ApJ*, 171, 565
Thompson, M.J., Christensen-Dalsgaard, J., Miesch, M.S., Toomre, J., 2003, *ARAA*, 41, 599
Vidotto, A.A., Gregory, S.G., Jardine, M., Donati, J.F., Petit, P., Morin, J., Folsom, C.P., Bouvier, J., Cameron, A.C., Hussain, G., Marsden, S., Waite, I.A., Fares, R., Jeffers, S., do Nascimento Jr, J.D., 2014, *MNRAS*, 441, 2361.
Wright, N.J., Drake, J.J., 2016, *Nature*, 535, 526
Wright, N.J., Drake, J.J., Mamajek, E.E., and Henry, W., 2011, *ApJ*, 743, 48
Wright, N.J., Newton, E.R., Williams, P.K.G., Drake, J.J., Yadav R.K., 2018 *NM-RAS*, 479, 2351